Implementation and Performance Analysis of 2D DFT Beamspace ESPRIT

Cherian P. Mathews[1] *Martin Haardt*[2] *Michael D. Zoltowski*[3]

[1] Department of Electrical Engineering, University of West Florida, 11000 University Parkway, Pensacola, FL 32514-5751
[2] Institute of Network Theory and Circuit Design, Technical University of Munich, D-80290 Munich, Germany
[3] School of Electrical Engineering, Purdue University, West Lafayette, IN 47907-1285

ABSTRACT

2D DFT Beamspace ESPRIT is a recently developed closed-form algorithm that provides automatically paired azimuth and elevation angle estimates of multiple sources incident on a uniform rectangular array of antennas. This paper shows how the performance of 2D DFT Beamspace ESPRIT can be improved via incorporation of null-steering. Null-steering provides the means for filtering out sources (interferers) in adjacent sectors, while searching for sources in a given spatial sector. Simulation results that document the performance improvement gained by null-steering are presented. The paper also analyzes the statistical performance of 2D DFT Beamspace ESPRIT. Asymptotic expressions for the variances of the 2D DFT Beamspace ESPRIT DOA estimates are obtained, and verified by computer simulations. The performance analysis results also apply to 2D Unitary ESPRIT, the element space counterpart of 2D DFT Beamspace ESPRIT.

1. INTRODUCTION

2D DFT Beamspace ESPRIT is a recently developed algorithm [1, 2], usable with uniform rectangular arrays (URAs), that provides automatically paired azimuth and elevation angle estimates of incident signals via a closed-form procedure. The algorithm is similar to *UCA-ESPRIT* [3] in that it does not require computationally expensive search procedures to obtain the direction-of-arrival (DOA) estimates, or ad-hoc pairing procedures to associate source bearing estimates relative to each of the array axes. Further, the algorithm does not break down if two (or more) sources have a common bearing relative to one of the array axes. *2D DFT Beamspace ESPRIT* thus overcomes the difficulties that characterize other 2D angle estimation algorithms. This paper discusses how null-steering can be employed to improve the performance of *2D DFT Beamspace ESPRIT*. The paper also analyzes the statistical performance of the algorithm.

2D DFT Beamspace ESPRIT can be applied in a reduced dimensional beamspace to perform parallel sector-wise searches for sources in different regions of space. This is effected by working with a subset of 2D DFT beams that have mainlobes in the spatial sector of interest. Several advantages such as reduced computational load, and reduced sensitivity to errors in the array model, are known to attend beamspace processing. We bring forth another advantage of beamspace processing with *2D DFT Beamspace ESPRIT*, namely the ability to place nulls at the locations of sources in neighboring sectors, while searching for sources in a given sector. This ability to filter out neighboring out-of-band sources improves the quality of the in-band source DOA estimates. Section 2 summarizes *2D DFT Beamspace ESPRIT*, and Section 3 describes how null-steering can be incorporated into the algorithm. The computer simulations of Section 5 demonstrate that significant improvements in estimator performance can be gained by employing null-steering in conjunction with *2D DFT Beamspace ESPRIT*.

The performance analysis of *2D DFT Beamspace ESPRIT* presented in Section 4 parallels the analysis of *UCA-ESPRIT* [3]. *2D DFT Beamspace ESPRIT* provides automatically paired DOA estimates via the eigenvalues of a matrix. The analysis yields expressions for the variances of the eigenvalues, and thus the variances of the DOA estimates. The performance analysis results also apply to *2D Unitary ESPRIT* [4], the element space counterpart of *2D DFT Beamspace ESPRIT*. The computer simulations of Section 5 show that the theoretical expressions for the DOA estimator variances are accurate; the empirical results are seen to closely follow the theoretical predictions.

2. SUMMARY OF 2D DFT BEAMSPACE ESPRIT

The array geometry involves a URA of $M \times N$ sensors located in the xy plane, with the array centroid located at the origin. The array elements parallel to the x axis are spaced a distance Δ_x apart, and those parallel to the y axis are spaced a distance Δ_y apart. The DOA of a source is specified by the pair (u, v), where $u = \sin\theta\cos\phi$ and $v = \sin\theta\sin\phi$ are the direction cosines with respect to the x and y axes, respectively. When a narrowband source (of wavelength λ) impinges on the array from the direction (u, v), the phase shifts between sucessive elements along the x and y axes are $\mu = 2\pi\frac{\Delta_x}{\lambda}u$ and $\nu = 2\pi\frac{\Delta_y}{\lambda}v$, respectively. Note that μ and ν lie in the range $[-\pi, \pi]$ when $\Delta_x = \Delta_y = \lambda/2$. The array output is modeled as $\mathbf{x}(t) = \mathbf{A}\mathbf{s}(t) + \mathbf{n}(t)$, where $\mathbf{x}(t)$ is the MN vector formed by stacking the columns of the URA outputs, $\mathbf{A}$ is the $MN \times d$ DOA matrix (assuming d incident sources), $\mathbf{s}(t)$ is the vector of signal complex envelopes at the origin, and $\mathbf{n}(t)$ is the stacked noise vector. The columns of $\mathbf{A}$ have the form $\text{vec}\,[\mathbf{a}_M(\mu)\mathbf{a}_N^T(\nu)]$, where $\text{vec}(\cdot)$ denotes the column stack-

1058-6393/96 $5.00 © 1996 IEEE
Proceedings of ASILOMAR-29

ing operator, and

$$\mathbf{a}_M(\mu) = e^{-j\frac{M-1}{2}\mu}[1, e^{j\mu}, \ldots, e^{j(M-1)\mu}]^T \quad (1)$$

is the centro-Hermitian version of the response vector of a M element uniform linear array. The *2D DFT Beamspace ESPRIT* algorithm is summarized below, and is followed by a brief explanation of pertinent points. In the summary, the symbol $\otimes$ denotes the Kronecker matrix product.

1. Average over K available snapshots to form the sample covariance matrix $\hat{\mathbf{R}}_{\mathbf{x}} = \frac{1}{K}\sum_{k=1}^{K}\mathbf{x}(k)\mathbf{x}^H(k)$.

2. Compute $\hat{\mathbf{R}} = \mathrm{Re}\{\mathbf{F}^H\hat{\mathbf{R}}_{\mathbf{x}}\mathbf{F}\}$, where $\mathbf{F}^H = \mathbf{W}_{B_y}^{(n)H} \otimes \mathbf{W}_{B_x}^{(m)H}$. A 2D DFT expedites this computation. The matrices $\mathbf{W}_{B_x}^{(m)}$ and $\mathbf{W}_{B_y}^{(n)}$ defined in (2) are chosen to provide coverage of the desired sector of (μ, ν) space.

3. Perform a real-valued eigenvalue decomposition (EVD) of $\hat{\mathbf{R}}$ and obtain an estimate of the number of sources, $\hat{d}$, in the sector. Obtain the beamspace signal subspace estimate $\hat{\mathbf{S}}$ via the $\hat{d}$ "largest" eigenvectors of $\hat{\mathbf{R}}$.

4. Obtain $\hat{\mathbf{\Psi}}_\mu$ and $\hat{\mathbf{\Psi}}_\nu$ as the least squares (or total least squares) solutions to the real-valued systems of equations $\mathbf{\Gamma}_{\mu 1}\hat{\mathbf{S}}\mathbf{\Psi}_\mu = \mathbf{\Gamma}_{\mu 2}\hat{\mathbf{S}}$, and $\mathbf{\Gamma}_{\nu 1}\hat{\mathbf{S}}\mathbf{\Psi}_\nu = \mathbf{\Gamma}_{\nu 2}\hat{\mathbf{S}}$. The $\mathbf{\Gamma}_{(\cdot)}$ matrices are defined in(4).

5. Perform an EVD of $\hat{\mathbf{\Psi}} = \hat{\mathbf{\Psi}}_\mu + j\hat{\mathbf{\Psi}}_\nu$. The eigenvalues of $\hat{\mathbf{\Psi}}$ are $\hat{\lambda}_i = \hat{\omega}_i + j\hat{\delta}_i$, where $\hat{\omega}_i = \tan(\hat{\mu}_i/2)$ and $\hat{\delta}_i = \tan(\hat{\nu}_i/2)$. The direction cosine estimates are thus $\hat{u}_i = \lambda/(\pi\Delta_x)\tan^{-1}(\hat{\omega}_i)$, and $\hat{v}_i = \lambda/(\pi\Delta_y)\tan^{-1}(\hat{\delta}_i)$.

The beamforming matrix $\mathbf{F}^H$ in step 2 synthesizes B_xB_y 2D DFT beams. B_x consecutive beams (beginning at beam $m \in [0, M-1]$) are formed along μ, and B_y consecutive beams (beginning at beam $n \in [0, N-1]$) are formed along ν. The 1D DFT beamforming matrices

$$\mathbf{W}_{B_x}^{(m)} = [\mathbf{a}_M(k_M m) \vdots \mathbf{a}_M(k_M(m+1)) \vdots \cdots \vdots \mathbf{a}_M(k_M(m+B_x-1))]$$

$$\mathbf{W}_{B_y}^{(n)} = [\mathbf{a}_N(k_N n) \vdots \mathbf{a}_N(k_N(n+1)) \vdots \cdots \vdots \mathbf{a}_N(k_N(n+B_y-1))] \quad (2)$$

where $k_M = (2\pi/M)$ and $k_N = (2\pi/N)$, are used to construct the 2D DFT beamforming matrix $\mathbf{F}^H$. The rows of $\mathbf{W}_{B_x}^{(m)H}$ are scaled M point DFT weight vectors corresponding to bins $m, m+1, \ldots, m+B_x-1$ (computed modulo M). The rows of $\mathbf{W}_{B_y}^{(n)H}$ have a similar interpretation. The beamformer $\mathbf{F}^H$ thus narrows the scope of the search for sources to the spatial sector roughly specified by $2\pi m/M \le \mu \le 2\pi(m+B_x-1)/M$, $2\pi n/N \le \nu \le 2\pi(n+B_y-1)/N$. Note also that a steering angle $\gamma > \pi$ (along μ or ν) is identical to the steering angle $\gamma - 2\pi$.

The equations in step 4 follow from a relationship between any two adjacent 2D DFT beams (adjacency in μ or ν). The matrices $\mathbf{\Gamma}_M^c$ and $\mathbf{\Gamma}_M^s$ defined below summarize these relationships. Row i of these matrices give the relationship between the ith and $i+1$st beams (modulo M).

$$\mathbf{\Gamma}_M^c = \begin{bmatrix} 1 & \cos\frac{\pi}{M} & 0 & \cdots & 0 & 0 \\ 0 & \cos\frac{\pi}{M} & \cos\frac{2\pi}{M} & \cdots & 0 & 0 \\ \vdots & \vdots & \vdots & \ddots & \vdots & \vdots \\ 0 & 0 & 0 & \cdots & \cos\frac{(M-2)\pi}{M} & \cos\frac{(M-1)\pi}{M} \\ -1^M & 0 & 0 & \cdots & 0 & \cos\frac{(M-1)\pi}{M} \end{bmatrix}$$

$$\mathbf{\Gamma}_M^s = \begin{bmatrix} 0 & \sin\frac{\pi}{M} & 0 & \cdots & 0 & 0 \\ 0 & \sin\frac{\pi}{M} & \sin\frac{2\pi}{M} & \cdots & 0 & 0 \\ \vdots & \vdots & \vdots & \ddots & \vdots & \vdots \\ 0 & 0 & 0 & \cdots & \sin\frac{(M-2)\pi}{M} & \sin\frac{(M-1)\pi}{M} \\ 0 & 0 & 0 & \cdots & 0 & \sin\frac{(M-1)\pi}{M} \end{bmatrix}$$

For reduced dimensional processing, form the submatrices

$$\mathbf{\Gamma}_1 = \mathbf{J}_{B_x-1}^{(m)}\mathbf{\Gamma}_M^c\mathbf{J}_{B_x}^{(m)T} \qquad \mathbf{\Gamma}_2 = \mathbf{J}_{B_x-1}^{(m)}\mathbf{\Gamma}_M^s\mathbf{J}_{B_x}^{(m)T}$$
$$\mathbf{\Gamma}_3 = \mathbf{J}_{B_y-1}^{(n)}\mathbf{\Gamma}_N^c\mathbf{J}_{B_y}^{(n)T} \qquad \mathbf{\Gamma}_4 = \mathbf{J}_{B_y-1}^{(n)}\mathbf{\Gamma}_N^s\mathbf{J}_{B_y}^{(n)T} \quad (3)$$

where $\mathbf{J}_{B_x}^{(m)}$ denotes a selection matrix that picks out B_x consecutive rows from the matrix it operates on (beginning with row m). Note again that the last row (row $M-1$) is followed by the first row (row 0). The matrices needed for step 4 are constructed as follows:

$$\mathbf{\Gamma}_{\mu 1} = \mathbf{I}_{B_y} \otimes \mathbf{\Gamma}_1 \qquad \mathbf{\Gamma}_{\mu 2} = \mathbf{I}_{B_y} \otimes \mathbf{\Gamma}_2$$
$$\mathbf{\Gamma}_{\nu 1} = \mathbf{\Gamma}_3 \otimes \mathbf{I}_{B_x} \qquad \mathbf{\Gamma}_{\nu 2} = \mathbf{\Gamma}_4 \otimes \mathbf{I}_{B_x} \quad (4)$$

2D Unitary ESPRIT [4, 2] is similar to *2D DFT Beamspace ESPRIT* except that it employs a different (sparse) transformation matrix $\mathbf{F}^H$ and, therefore, also different selection matrices instead of the $\mathbf{\Gamma}_{(\cdot)}$ of step 4, and that these matrices have full dimension (reduced dimensional beamspace processing is not possible). Due to these similarites, the performance analysis results developed in Section 4 are easily modified to encompass *2D Unitary ESPRIT*.

3. INCORPORATING NULL-STEERING INTO 2D DFT BEAMSPACE ESPRIT

As described above, *2D DFT Beamspace ESPRIT* allows for sectorization of the search space via 2D DFT beamforming, and provides closed-form DOA estimates of sources in the sector of interest. To illustrate, consider an 8×8 URA. *2D DFT Beamspace ESPRIT* could employ nine beams (a 3×3 subset of 2D DFT beams), with nine such overlapping beam sets spannning the entire arrival angle space. The algorithm is computationally efficient and requires only a real-valued 9×9 EVD per sector (as opposed to a 64×64 EVD for element-space operation).

The maximum number of sources that *2D DFT Beamspace ESPRIT* can resolve per sector is equal to the number of independent equations in step 4 of the algorithm summary. The algorithm can thus resolve a maximum of six sources per sector in the nine beam example presented

above. This figure of six sources per sector may be optimistic, since sources from adjacent sectors can leak into the current one (due to the high sidelobes of the 2D DFT beams), thereby increasing the effective number of sources in the current sector. The development below shows how null-steering can be employed to alleviate the problem of source leakage from adjacent sectors into the current one. A simple procedure for steering upto two independent nulls in the directions of sources (interferers) in adjacent sectors is described.

With the 1D beamformers as defined in (2), the 2D DFT beam steered to ($\mu_s = k_M m, \nu_s = k_N n$) has the response

$$b_{m,n}(\mu,\nu) = \frac{\sin\left[\frac{M}{2}(\mu - k_M m)\right]}{\sin\left[\frac{1}{2}(\mu - k_M m)\right]} \cdot \frac{\sin\left[\frac{N}{2}(\nu - k_N n)\right]}{\sin\left[\frac{1}{2}(\nu - k_N n)\right]} \quad (5)$$

This pattern has a null if $\mu = k_M i$, $i \in [0, M-1]$, or $\nu = k_N j$, $j \in [0, N-1]$, except that it has a peak if $(\mu,\nu) = (k_M m, k_N n)$. A 2D DFT beam steered to ($\mu_s = k_M m + \alpha, \nu_s = k_N n + \beta$) can be generated just as easily as the beam of (5). The resulting beampattern

$$\overline{b}_{m,n}(\mu,\nu) = \frac{\sin\left[\frac{M}{2}(\mu - k_M m - \alpha)\right]}{\sin\left[\frac{1}{2}(\mu - k_M m - \alpha)\right]} \cdot \frac{\sin\left[\frac{N}{2}(\nu - k_N n - \beta)\right]}{\sin\left[\frac{1}{2}(\nu - k_N n - \beta)\right]} \quad (6)$$

has a null if $\mu = k_M i + \alpha$, $i \in [0, M-1]$ or $\nu = k_N j + \beta$, $j \in [0, N-1]$, except that it has a peak if $(\mu,\nu) = (k_M m + \alpha, k_N n + \beta)$. Now $\alpha \in (-\pi/M, \pi/M)$ and $\beta \in (-\pi/N, \pi/N)$ can be chosen so as to provide nulls at the locations of two sources in adjoining sectors (α provides a null at the μ location of the first interferer, and β provides a null at the ν location of the second). Due to the breakdown of the search space into sectors, information on the locations of sources in adjacent sectors is available when searching for sources in the next sector. Appropriate values for the angle shifts α and β are thus available.

Null-steering as described above is easily incorporated into *2D DFT Beamspace ESPRIT*. Given values for α and β, we form the 1D DFT beamforming matrices

$$\begin{aligned} \overline{\mathbf{W}}_{B_x}^{(m)} &= \text{diag}\{\mathbf{a}_M(\alpha)\}\mathbf{W}_{B_x}^{(m)} \\ \overline{\mathbf{W}}_{B_y}^{(n)} &= \text{diag}\{\mathbf{a}_N(\beta)\}\mathbf{W}_{B_y}^{(n)} \end{aligned} \quad (7)$$

where $\mathbf{a}_M$ and $\mathbf{W}$ are defined in (1) and (2), respectively. The matrices of (7) synthesize 2D DFT beams with nulls at the desired locations, and are employed in step 2 of the algorithm summary. The resulting beampatterns (6) are spatially shifted versions of the original beams (5). The beamspace relationships described by the $\mathbf{\Gamma}_{(.)}$ matrices in step 4 of the algorithm thus hold provided the source DOA is considered to be $(\mu - \alpha, \nu - \beta)$. Thus in the final stage (step 5), the algorithm provides estimates $\overline{u}$ and $\overline{v}$, where the true direction cosine estimates are $u = \overline{u} + \alpha$ and $v = \overline{v} + \beta$. The modifications needed to incorporate null-steering into *2D DFT Beamspace ESPRIT* are summarized below.

- Choose α and β to provide nulls at locations of sources (interferers) in adjacent sectors.
- Form the 1D DFT beamforming matrices of (7) and employ them in step 2 of *2D DFT Beamspace ESPRIT*.
- The source DOAs are given by $\mu = \overline{\mu} + \alpha$ and $\nu = \overline{\nu} + \beta$, where $\overline{\mu}$ and $\overline{\nu}$ are the estimates obtained from step 5 of *2D DFT Beamspace ESPRIT*.

4. PERFORMANCE ANALYSIS RESULTS

The analysis of *2D DFT Beamspace ESPRIT* presented below follows the analysis of *UCA-ESPRIT* [3]. The development of *2D DFT Beamspace ESPRIT* shows that the error free matrix $\mathbf{\Psi} = \mathbf{\Psi}_\mu + j\mathbf{\Psi}_\nu$ has the spectral decomposition $\mathbf{\Psi} = \mathbf{T}^{-1}(\mathbf{\Omega}_\mu + j\mathbf{\Omega}_\nu)\mathbf{T}$, where $\mathbf{T}$ is real-valued. Thus $\mathbf{\Psi}_\mu$ and $\mathbf{\Psi}_\nu$ have a common set of real-valued eigenvectors given by the columns of $\mathbf{T}^{-1}$. $\mathbf{\Omega}_\mu + j\mathbf{\Omega}_\nu$ is the diagonal matrix whose elements are the eigenvalues $\lambda_i = \omega_i + j\delta_i$. In the following developments, the left and right eigenvectors of $\mathbf{\Psi}$ are denoted $\mathbf{q}_i^T$ and $\mathbf{x}_i$, respectively. A superscript e denotes the error in an estimate, and a superscript $\dagger$ denotes the Moore-Penrose pseudo-inverse. The statistics of the signal eigenvectors $\hat{\mathbf{s}}_i$ (columns of $\hat{\mathbf{S}}$) are required for the analysis. Lemma 1 drawn from [3] gives these statistics. The columns of the matrix $\mathbf{G}$ in Lemma 1 are the noise eigenvectors of $\mathbf{R}$, l_i, $1 \le i \le d$ denote the d largest eigenvalues (assumed distinct) of $\mathbf{R}$, and σ is the noise power (the noise is assumed to be Gaussian, and spatially white).

Lemma 1 *The signal eigenvector estimation errors $\mathbf{s}_i^e$ are asymptotically (for large number of snapshots K) zero mean with covariance matrices given by*

$$Cov(\mathbf{s}_i^e, \mathbf{s}_j^e) = E\left[\mathbf{s}_i^e \mathbf{s}_j^{eT}\right] =$$

$$\frac{1}{K}\left[\sum_{\substack{r=1 \\ r\neq i}}^{d}\sum_{\substack{s=1 \\ s\neq j}}^{d} \frac{\Gamma_{rsji}}{(l_i - l_r)(l_j - l_s)}\mathbf{s}_r\mathbf{s}_s^T + \frac{l_i\sigma}{2(l_i - \sigma)^2}\mathbf{G}\mathbf{G}^T\delta_{ij}\right]$$

where

$$\begin{aligned} \Gamma_{rsji} &= \frac{1}{2}\left\{l_i l_s \delta_{ij}\delta_{rs} + l_i l_j \delta_{is}\delta_{jr} + \mathbf{w}_r^T(\mathbf{s}_s\mathbf{s}_j^T + \mathbf{s}_j\mathbf{s}_s^T)\mathbf{w}_i\right\} \\ \mathbf{w}_i &= Im\{\mathbf{F}^H\mathbf{R}_x\mathbf{F}\}\mathbf{s}_i. \end{aligned}$$

The following theorem gives asymptotic expressions for the variances/covariance of the *2D DFT Beamspace ESPRIT* estimators $\hat{\omega}_i$ and $\hat{\delta}_i$. The fact that $\hat{\omega}_i$ and $\hat{\delta}_i$ are concentrated about their true values is used to obtain approximate expressions for the variances of the direction cosine estimators $\hat{u}_i$ and $\hat{v}_i$. The theorem can be proved along the lines of a similar theorem in [3].

Theorem 1 *The* 2D DFT Beamspace ESPRIT *estimators $\hat{\omega}_i$ and $\hat{\delta}_i$ are asymptotically unbiased. Asymptotic expressions for their variances/covariance are as follows:*

$$\begin{aligned} Var(\hat{\omega}_i) &= \boldsymbol{\alpha}_{iR}^T \mathbf{H}_i \boldsymbol{\alpha}_{iR} \\ Var(\hat{\delta}_i) &= \boldsymbol{\alpha}_{iI}^T \mathbf{H}_i \boldsymbol{\alpha}_{iI} \\ Cov(\hat{\omega}_i, \hat{\delta}_i) &= \boldsymbol{\alpha}_{iR}^T \mathbf{H}_i \boldsymbol{\alpha}_{iI}, \text{ where} \end{aligned} \quad (8)$$

$$\begin{aligned} \mathbf{H}_i &= \sum_{j=1}^{d}\sum_{k=1}^{d} \mathbf{x}_{ij}\mathbf{x}_{ik}\, Cov(\mathbf{s}_j^e, \mathbf{s}_k^e) \\ \boldsymbol{\alpha}_{iR}^T &= \mathbf{q}_i^T(\mathbf{\Gamma}_{\mu 1}\mathbf{S})^\dagger(\mathbf{\Gamma}_{\mu 2} - \omega_i\mathbf{\Gamma}_{\mu 1}) \\ \boldsymbol{\alpha}_{iI}^T &= \mathbf{q}_i^T(\mathbf{\Gamma}_{\nu 1}\mathbf{S})^\dagger(\mathbf{\Gamma}_{\nu 2} - \delta_i\mathbf{\Gamma}_{\nu 1}) \end{aligned}$$

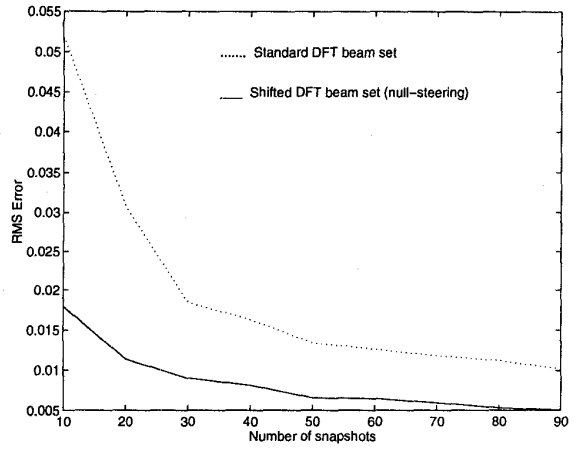

Figure 1: RMS estimation error for source 1

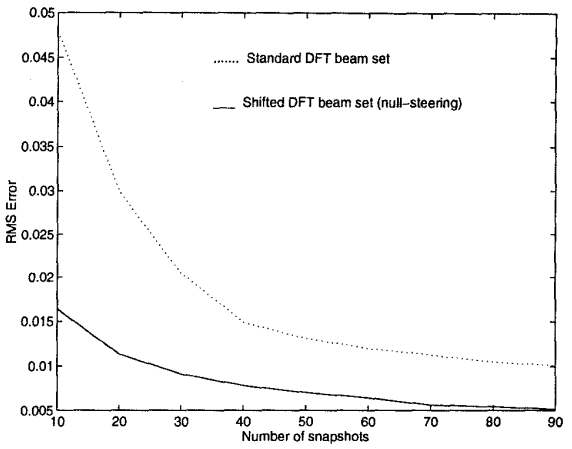

Figure 2: RMS estimation error for source 2

The direction cosine estimator variances are given by

$$Var\,(\hat{u}_i) \approx \left[\frac{\lambda}{\pi\Delta_x(1+\omega^2)}\right]^2 Var\,(\hat{\omega}_i) \qquad (9)$$

$$Var\,(\hat{v}_i) \approx \left[\frac{\lambda}{\pi\Delta_y(1+\delta^2)}\right]^2 Var\,(\hat{\delta}_i)$$

5. RESULTS OF COMPUTER SIMULATIONS

Results of computer simulations that demonstrate the efficacy of null-steering with *2D DFT Beamspace ESPRIT* are presented below. Simulation results that verify the theoretical performance analysis results are also presented. All simulations employ an 8×8 URA (*i. e.* , $M = N = 8$) with an interelement spacing of half a wavelength in both x and y directions. The signal to noise ratios (SNR's) referred to in the following developments are per source per array element. The rms error (RMSE) is employed as the performance metric. The RMSE of the *i-th* source is computed as follows:

$$\hat{RMSE}_i = \sqrt{\frac{1}{T}\sum_{t=1}^{T}\{(\hat{u}_{i_t}-u_i)^2+(\hat{v}_{i_t}-v_i)^2\}}, \qquad (10)$$

where $(\hat{u}_{i_k}, \hat{v}_{i_k})$ are the coordinate estimates of the *i-th* source in the *k-th* trial, and T is the total number of trials.

Efficacy of Null-Steering

The source scenario includes four uncorrelated sources located at $(u_1, v_1) = (-1/8, -1/8)$, $(u_2, v_2) = (1/8, 1/8)$, $(u_3, v_3) = (-5/8, 0)$, and $(u_4, v_4) = (0, 5/8)$, where u_i and v_i are the direction cosines of the *i-th* source relative to the x and y axes, respectively. We consider a 3×3 beam set of nine standard DFT beams, and a 3×3 set of shifted DFT beams that steer nulls in the directions of interferers. The standard DFT beam set is centered at $(u, v) = (0, 0)$. Sources 1 and 2 lie within the main-lobes of this beam set, and are considered in-band sources. Sources 3 and 4 (out-of-band sources) lie in adjacent sectors and are positioned at the first side-lobe peaks of the closest beams of the standard DFT beam set. These sources leak into the current sector, effectively increasing the number of sources in the sector to four. The shifted DFT beam set is chosen to provide nulls at the locations of sources 3 and 4. Accordingly, this beam set is centered at $(u, v) = (1/8, -1/8)$ (the corresponding angle shifts referred to in the null-steering development are $\alpha = \pi/8$ and $\beta = -\pi/8$).

Simulations were performed to assess the quality of the *2D DFT Beamspace ESPRIT* estimates of the in-band sources (with and without null-steering,) as the number of snapshots K was varied. In the simulations, the in-band sources had SNRs of -5dB each, while the out-of-band sources had SNRs of 0dB each. The sensor noise was complex-Gaussian distributed, and was spatially and temporally white. Sample estimator statistics were obtained using $T = 500$ independent trials. Fig. 1 shows that while employing the standard DFT beam set, the RMSE of source 1 rises dramatically if the number of snapshots drops below 40. In contrast, the figure shows that low RMSEs are achieved if null-steering is employed, even if the number of snapshots drops as low as 10. Examination of Fig. 2 shows that similar results hold for the second in-band source. The simulations thus show that null-steering greatly enhances estimator performance in low information to noise scenarios. We also note that incorporation of null-steering can enable *2D DFT Beamspace ESPRIT* to operate in a lower dimensional beamspace (leading to reduced computational demands) than would otherwise be possible. This is because sources in adjacent sectors can be filtered out, thereby keeping down the effective number of sources in the sector of interest.

Verification of Performance Analysis Results

The source scenario consists of $d = 3$ equi-powered, uncorrelated sources located at $(u_1, v_1) = (0, 0)$, $(u_2, v_2) = (1/8, 0)$, and $(u_3, v_3) = (0, 1/8)$. Sources 1 and 2 are separated by a half-beamwidth, *i. e.*, half the Rayleigh resolution limit, as are sources 2 and 3. Sources 1 and 2 have the same v coordinate, while sources 1 and 3 have the same u coordinate. $K = 64$ snapshots were employed in the simulations, and sample performance statistics were computed

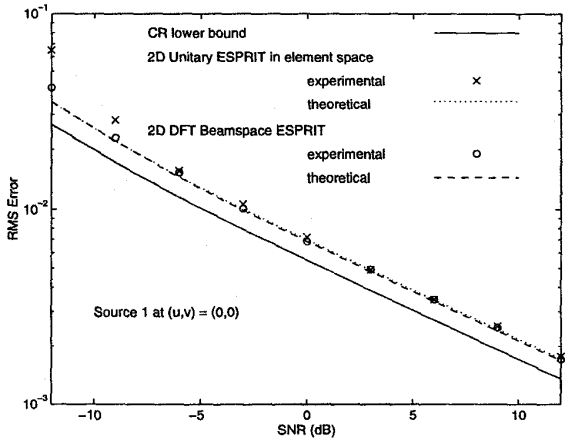

Figure 3: Performance curves for source 1.

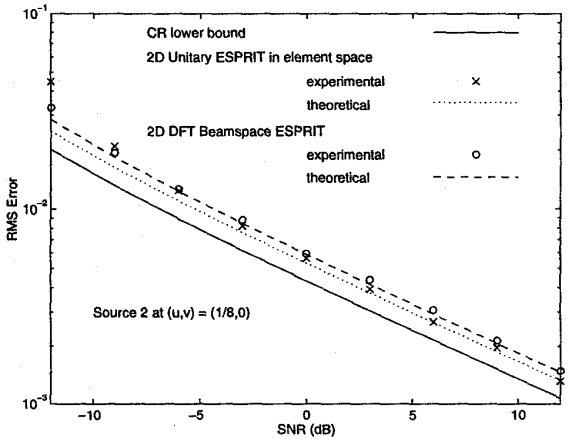

Figure 4: Performance curves for source 2.

from $T = 1000$ independent trials. The sensor noise was spatially and temporally white Gaussian noise, as in the previous simulation example.

The simulations employed a standard 3×3 2D DFT beam set centered at $(u, v) = (0, 0)$. The simulations investigated the performance of *2D DFT Beamspace ESPRIT* and *2D Unitary ESPRIT* as a function of SNR. The RMSE's of the *2D DFT Beamspace ESPRIT* estimates and the *2D Unitary ESPRIT* estimates for sources 1, 2, and 3 are plotted together with the theoretical performance curves in Figures 3,4, and 5, respectively. The ultimate performance dictated by the Cramer Rao bound is also depicted. The figures show that the empirical RMSEs closely follow the theoretical predictions, except for slight deviations at low SNRs. We also see that the performance of *2D DFT Beamspace ESPRIT* is comparable to that of *2D Unitary ESPRIT*. However, the computational demands of *2D DFT Beamspace ESPRIT* are significantly lower than those of *2D Unitary ESPRIT*. The former is a beamspace algorithm requiring 9×9 EVDs in the above source scenario, whereas the latter is an element space algorithm that requires 64×64 EVDs in the same source scenario.

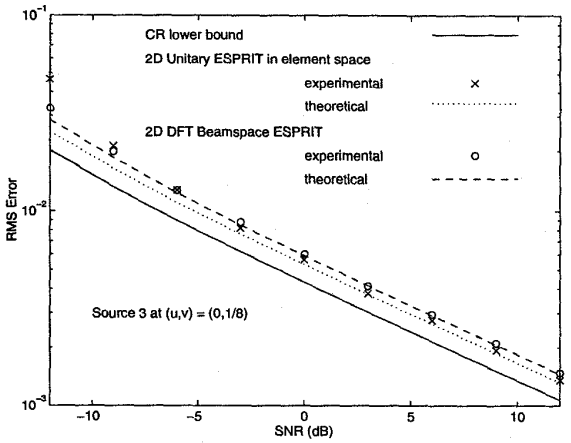

Figure 5: Performance curves for source 3.

6. SUMMARY

2D DFT Beamspace ESPRIT is a recently developed algorithm [1] that provides automatically paired azimuth and elevation angle estimates of signals incident on a uniform rectangular antenna array via a closed-form procedure. This paper describes how the performance of *2D DFT Beamspace ESPRIT* can be improved by incorporating null-steering into the algorithm. Independent nulls can be steered in the directions of two sources outside the spatial sector of interest, thereby improving the quality of the in-band source estimates. The paper also analyzes the statistical performance of 2D DFT Beamspace ESPRIT. Asympotic expressions for the 2D DFT Beamspace ESPRIT DOA estimator variances are obtained and verified by computer simulations.

REFERENCES

[1] M.D. Zoltowski, M. Haardt, and C.P. Mathews, "Closed-form 2D angle estimation with rectangular arrays via DFT Beamspace ESPRIT", in *28th Asilomar IEEE Conference on Signals, Systems, and Computers*, 1994, pp. 682–687.

[2] M.D. Zoltowski, M. Haardt, and C.P. Mathews, "Closed-form 2D angle estimation with rectangular arrays in element space or beamspace via Unitary ESPRIT", *to appear in IEEE Trans. on Signal Processing*, February 1996.

[3] C.P. Mathews and M.D. Zoltowski, "Performance analysis of the UCA-ESPRIT algorithm for circular ring arrays", *IEEE Trans. on Signal Processing*, vol. 42, pp. 2535–2539, September 1994.

[4] M. Haardt, M.D. Zoltowski, C.P. Mathews, and J.A. Nossek, "2D Unitary ESPRIT for efficient 2D parameter estimation", in *Proc. IEEE Int. Conf. Acoust., Speech, Signal Processing*, 1995, pp. 2096–2099.